

A Fifth-Order Low-Dissipative Conservative Upwind Compact Scheme Using Centered Stencil

Conghai Wu^{1,2,*}, Sujuan Yang³ and Ning Zhao²

¹ State Key Laboratory of Aerodynamics, Mianyang 621000, China

² College of Aerospace Engineering, Nanjing University of Aeronautics and Astronautics, Nanjing 210016, China

³ College of Science, PLA University of Science and Technology, Nanjing 211101, China

Received 15 October 2012; Accepted (in revised version) 29 December 2013

Available online 17 September 2014

Abstract. In this paper, a conservative fifth-order upwind compact scheme using centered stencil is introduced. This scheme uses asymmetric coefficients to achieve the upwind property since the stencil is symmetric. Theoretical analysis shows that the proposed scheme is low-dissipative and has a relatively large stability range. To maintain the convergence rate of the whole spatial discretization, a proper non-periodic boundary scheme is also proposed. A detailed analysis shows that the spatial discretization implemented with the boundary scheme proposed by Pirozzoli [J. Comput. Phys., 178 (2001), pp. 81–117] is approximately fourth-order. Furthermore, a hybrid methodology, coupling the compact scheme with WENO scheme, is adopted for problems with discontinuities. Numerical results demonstrate the effectiveness of the proposed scheme.

AMS subject classifications: 65M06, 76M20, 76Q05

Key words: High-order scheme, compact scheme, conservative scheme, low-dissipative scheme.

1 Introduction

In recent years, high-order compact schemes have attracted much attention in various fields, such as simulation of incompressible or compressible flows, computational aeroacoustics, and computational electromagnetics [1–4]. Compact schemes can be viewed as weighted averages of explicit difference schemes at several adjacent points. Hence, these schemes are implicit ones and often produce tri-diagonal or penta-diagonal linear systems which could be solved by many effective algorithms. Compared with those explicit finite difference schemes, compact schemes use narrower stencil and show better spectral resolution property when offering the same order of approximation. Therefore, for

*Corresponding author.

Email: wrainment@163.com (C. H. Wu), zhaoam@nuaa.edu.cn (N. Zhao)

problems with wide range of spatial and temporal scales, compact schemes should be a good choice. For such multi-scale problems, spectral methods may do the best. However, they are used mostly for problems with simple geometries and boundary conditions. Another type of difference schemes, the dispersion-relation-preserving (DRP) schemes, optimizes the coefficients of the schemes in order to resolve short waves whose wavelength is small with respect to the computational grid [5]. Since for long waves even lower order scheme can do fairly well, DRP schemes can be another choice for the problems mentioned above. However, they perform poorly for longer distances of travel if optimization is too aggressive [6].

A systematic analysis to high-order accurate, central stencil schemes appropriate for problems with a wide range of scales was presented by Lele [7]. However, for advection dominated problems, central high-order compact schemes lack some robustness because there is no built-in dissipation term in the schemes. A filtering procedure could be used to cure this problem. Otherwise, an artificial viscosity term has to be added into the scheme to improve the robustness of the scheme. Another choice is using upwind schemes which have inherent dissipation. Since difference schemes usually achieve the highest convergence order on their grid stencils and no effort has been made to optimize the resolution properties, the stencils used by upwind compact schemes are often upwind biased [8,9]. However, there are some researches about upwind schemes using centered stencils [10,11], whose coefficients are no longer symmetric. Compared with the central schemes on the same stencils, these schemes are usually degraded by one convergence order, and a free parameter is left to optimize the resolution property.

For problems involving discontinuities, compact schemes mentioned above will produce oscillations whose amplitude does not decrease when the grid is refined. To overcome this difficulty, nonlinear procedures should be employed. One way is to modify the compact schemes by using the ideas of TVD, WENO [12], or other kinds of limiter [13]. Hybridization with shock capturing schemes could be another kind of ways which take into account high resolution, high efficiency and good robustness. There are some works about hybrid compact ENO/WENO schemes [11,14,15], among which the hybrid methodology of Ren et al. shows the best resolution [16,17].

The compact schemes proposed by Lele [7] need special boundary treatment to maintain the global conservation. However, conservative compact schemes guarantee the conservation without additional treatment [14]. Furthermore, the shock capturing schemes are usually conservative which is necessary for converging to the right solution when the grid is refined. Therefore, it should be better to use a conservative scheme for hybridization with shock capturing schemes. But the order of boundary treatment of conservative schemes should be analyzed carefully because the two adjacent fluxes of the boundary point may employ different schemes, which will be shown in the present work.

In this paper, a set of conservative upwind compact schemes with a free parameter using a centered stencil are given firstly. Following the method in [10], this free parameter is set to satisfy the condition that the dissipation errors of the compact scheme are smaller or comparable to the corresponding phase errors. Next, the boundary treatment is given

to maintain the convergence rate of the inner scheme. After that, the stability property of the spatial discretization and the whole discretization including the time integration are analyzed. Then, the hybridization method of the proposed scheme with WENO scheme is introduced for problems with discontinuities. At last, the numerical investigation is performed, where the high accuracy and the low-dissipation property of the proposed scheme are demonstrated.

2 A fifth-order conservative compact scheme

2.1 Conservative compact scheme

Conservative compact schemes have advantages over those non-conservative counterparts in the following two aspects. The first is that they need no special treatment to maintain the global conservation, and the other is that it may be a better choice for coupling with shock capturing schemes than those non-conservative ones. In this subsection, the formulation of conservative approximations to the derivative of a scalar variable $u(x)$ from point-wise values is given.

Consider a scalar variable $u(x)$ and a uniform grid $x_i = ih$, $i = 1, 2, \dots, N$, where h is the grid length. Let

$$u_i = u(x_i), \quad i = 1, 2, \dots, N.$$

To get a conservative approximation to $u'(x)$ at node x_i , the problem is to determine the numerical flux at the intermediate node. Suppose that the approximation to $u'(x)$ is k -th order accurate, that is

$$\frac{1}{h}(\tilde{u}_{i+1/2} - \tilde{u}_{i-1/2}) = u'(x_i) + \mathcal{O}(h^k), \quad i = 1, 2, \dots, N, \quad (2.1)$$

where $\tilde{u}_{i+1/2}$ and $\tilde{u}_{i-1/2}$ are the numerical fluxes which need to be determined.

In order to analyze the relation between the formula of numerical flux and the convergence order of Eq. (2.1), a function $s(x)$ is considered which is given implicitly by

$$u(x) = \frac{1}{h} \int_{x-h/2}^{x+h/2} s(\xi) d\xi. \quad (2.2)$$

Differentiating this equality at x_i , we have

$$u'(x_i) = \frac{1}{h}(s_{i+1/2} - s_{i-1/2}), \quad (2.3)$$

where $s_{i+1/2} = s(x_{i+1/2})$. A k -th order approximation to $s_{i+1/2}$ can meet the condition of Eq. (2.1) in most cases:

$$\tilde{u}_{i+1/2} = s(x_{i+1/2}) + \mathcal{O}(h^k). \quad (2.4)$$

It seems that an $\mathcal{O}(h^{k+1})$ term is needed to satisfy Eq. (2.1). In practice, the $\mathcal{O}(h^k)$ term is usually smooth. Hence, the difference in Eq. (2.1) would give an extra h , just to cancel the one in the dominator. However, the smooth property of the $\mathcal{O}(h^k)$ term will be violated when two adjacent fluxes use different kind of schemes, resulting in degradation of the convergence accuracy. This could happen at the boundary treatment which will be discussed later.

Now we will construct the numerical flux which should meet the condition of Eq. (2.1). A compact reconstruction of $u(x)$ around the intermediate node $x_{i+1/2}$ can be written as:

$$\sum_{l=-L_1}^{L_2} a_l \tilde{u}_{i+1/2+l} = \sum_{m=-M_1}^{M_2} b_m u_{i+m}. \quad (2.5)$$

Assuming that the function $s(x)$ can be expanded in Taylor series up to order k ,

$$s(x) = \sum_{n=0}^{k-1} s^{(n)}(x_{i+1/2}) \frac{(x-x_{i+1/2})^n}{n!} + \mathcal{O}(h^k).$$

Let Eq. (2.4) hold, then

$$\begin{aligned} \tilde{u}_{i+1/2+l} &= s(x_{i+1/2+l}) + \mathcal{O}(h^k) = \sum_{n=0}^{k-1} s^{(n)}(x_{i+1/2}) \frac{(x_{i+1/2+l}-x_{i+1/2})^n}{n!} + \mathcal{O}(h^k) \\ &= \sum_{n=0}^{k-1} s^{(n)}(x_{i+1/2}) \frac{l^n}{n!} h^n + \mathcal{O}(h^k). \end{aligned} \quad (2.6)$$

According to the definition of function $s(x)$, we have

$$u_{i+m} = \frac{S_{i+m+1/2} - S_{i+m-1/2}}{h},$$

where $S(x)$ is one of the primitive function of $s(x)$,

$$S(x) = \sum_{n=0}^{k-1} s^{(n)}(x_{i+1/2}) \frac{(x-x_{i+1/2})^{n+1}}{(n+1)!} + \mathcal{O}(h^{k+1}).$$

Thus,

$$u_{i+m} = \sum_{n=0}^{k-1} s^{(n)}(x_{i+1/2}) \frac{1}{(n+1)!} [m^{n+1} - (m-1)^{n+1}] + \mathcal{O}(h^k). \quad (2.7)$$

Replacing \tilde{u} and u in Eq. (2.5) with the Taylor series expansions, and matching the coefficients of powers of h up to k -th order, we get

$$(n+1) \sum_{l=-L_1}^{L_2} a_l l^n - \sum_{m=-M_1}^{M_2} b_m [m^{n+1} - (m-1)^{n+1}] = 0, \quad n=0, \dots, k-1. \quad (2.8)$$

Then, the coefficients of the compact scheme can be obtained by solving Eq. (2.8).

2.2 A fifth-order conservative compact scheme

In the previous subsection, the general formula of the conservative compact scheme is given. With this formula, a fifth-order conservative compact scheme will be constructed in this subsection. Here the case $L_1 = L_2 = M_1 = 1$, $M_2 = 2$ is considered which means that the stencil is symmetric. According to Eq. (2.8), there are $L_1 + L_2 + 1 + M_1 + M_2 + 1 = 7$ unknown coefficients and only six of them are independent (one could set any coefficient to be 1). Let the order requirement be $k = 5$, a set of one-parameter fifth-order compact schemes can be obtained as

$$\begin{aligned} & (12 - 6\alpha)\tilde{u}_{i-1/2} + 36\tilde{u}_{i+1/2} + (12 + 6\alpha)\tilde{u}_{i+3/2} \\ & = (1 - \alpha)u_{i-1} + (29 - 9\alpha)u_i + (29 + 9\alpha)u_{i+1} + (1 + \alpha)u_{i+2}. \end{aligned} \quad (2.9)$$

The only sixth-order compact scheme is achieved when $\alpha = 0$ which is a central scheme without built-in dissipation. The compact scheme using upwind biased stencil can also be achieved when $\alpha = \pm 1$, where the sign is chosen by the upwind direction. This is the scheme extensively analyzed by Pirozzoli [14] which shows good resolution property. But sometimes it may be somewhat dissipative. However, α could be chosen such that the scheme is robust and is less dissipative than the scheme using an upwind-biased stencil.

Here the resolution property of Eq. (2.9) will be analyzed. Consider a monochromatic wave with a scaled wavenumber κ

$$f(x) = e^{i\kappa x/h}.$$

The first derivative of f will be

$$f' = \frac{i\kappa}{h} e^{i\kappa x/h} = \frac{i\kappa}{h} f.$$

For difference scheme, we could get a formula in a similar form as below

$$\tilde{f}' = \frac{i\tilde{\kappa}}{h} f,$$

where \tilde{f}' is the numerical approximation to the first order derivative, and $\tilde{\kappa}$ is the effective wavenumber which can be viewed as an approximation to κ . For the scheme in Eqs. (2.1)-(2.9),

$$\tilde{\kappa} = 2 \sin \frac{\kappa}{2} \frac{\sum_{m=-M_1}^{M_2} b_m e^{im\kappa}}{\sum_{l=-L_1}^{L_2} a_l e^{i(l+1/2)\kappa}}. \quad (2.10)$$

$\tilde{\kappa}$ will be used for measuring the dissipation and dispersion error of the scheme. Here, the linear advection equation is considered

$$\frac{\partial u}{\partial t} + c \frac{\partial u}{\partial x} = 0, \quad a \leq x \leq b, \quad (2.11)$$

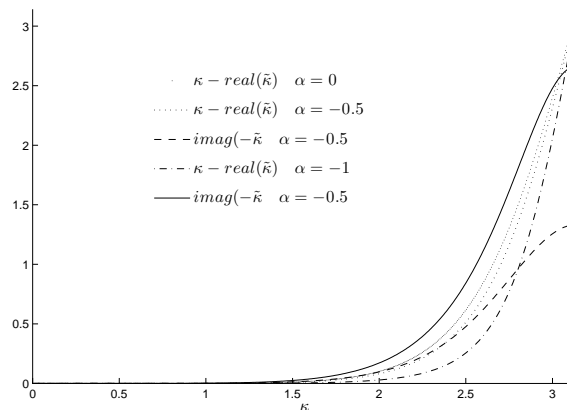


Figure 1: Phase errors and dissipation errors with several values of α . The three solid lines from top to bottom correspond to the phase errors of the schemes using α values of 0, -0.5 and -1 , respectively.

where $c > 0$. Let the initial condition be $u(x, 0) = f(x) = e^{ikx/h}$. Then the exact solution will be

$$u(x, t) = f(x - ct) = e^{i\kappa(x-ct)/h} = e^{i(\kappa x - c\kappa t)/h}. \tag{2.12}$$

If the scheme in Eqs. (2.1)-(2.9) is employed as the spatial discretization and the temporal discretization error is ignored, the solution will be

$$\tilde{u}(x, t) = e^{i(\kappa x - c\tilde{\kappa}t)/h}. \tag{2.13}$$

Compared this solution with the exact solution, the only difference is that one of the variant κ is replaced by $\tilde{\kappa}$. Moreover, the real part and the imaginary part of the difference between $\tilde{\kappa}$ and κ will lead to the dispersive and dissipative error respectively. Here the real part and the imaginary part of $\tilde{\kappa} - \kappa$ will be used to indicate the dimensionless dispersive and dissipative error. Since the imaginary part of κ is always zero for $0 \leq \kappa \leq \pi$ and positive error values are expected to be shown in the figure, these two errors are indicated by $\kappa - \text{real}(\tilde{\kappa})$ and $\text{imag}(-\tilde{\kappa})$ respectively.

Fig. 1 shows the dispersion and dissipation errors of (4) with α at 0, -0.5 and -1 . The imaginary part of $\tilde{\kappa}$ vanishes for $\alpha = 0$, which is not shown in the figure. Note that α should be negative such that the difference scheme is upwind biased. As the value of α decreases, the dissipation errors of the schemes will increase. Following the idea in [10], the case that the dissipation errors of the scheme are smaller or comparable to the dissipation error is considered. From this figure, this condition can be fulfilled by $-0.5 < \alpha < 0$. Because some dissipation is necessary for the robustness of the scheme, a balanced value of $\alpha = -0.5$ is chosen in this paper. This scheme can be written as

$$15\tilde{u}_{i-1/2} + 36\tilde{u}_{i+1/2} + 9\tilde{u}_{i+3/2} = \frac{3}{2}u_{i-1} + \frac{67}{2}u_i + \frac{49}{2}u_{i+1} + \frac{1}{2}u_{i+2}. \tag{2.14}$$

3 Boundary treatment and time discretization

3.1 Boundary treatment

For non-periodic problem, a proper boundary scheme should be implemented which is crucial to the formal order of and the stability of the whole scheme. It is sufficient to maintain the convergence rate of the inner scheme with a one-order lower boundary scheme [18]. Therefore, a fourth-order approximation at boundary points could be utilized.

For compact scheme, the boundary schemes may not be the same as inner schemes even if enough ghost points are used. Therefore, as mentioned in the previous section, the boundary scheme may be suffered from a degradation of convergence order. Because of implicit nature of the inner compact schemes, the analysis of the accuracy order of the boundary treatment will be inconvenient. The following analysis is based on the conservative explicit scheme and only has some reference significance to conservative compact scheme. But the numerical investigation in later section validates the conclusion.

For example, let the grid nodes be x_1, x_2, \dots, x_N . To get the numerical derivative of the left boundary point x_1 , the numerical fluxes $\tilde{u}_{1/2}$ and $\tilde{u}_{3/2}$ should be given. Suppose that these two fluxes meet the following equations

$$\tilde{u}_{1/2} = S_{1/2} + \mathcal{O}(h^4), \quad \tilde{u}_{3/2} = S_{3/2} + \mathcal{O}(h^5),$$

where the formula of $\tilde{u}_{1/2}$ is the boundary treatment and that of $\tilde{u}_{3/2}$ is the inner scheme. This boundary treatment is usually considered as a fourth-order accurate scheme and the inner scheme is fifth-order accurate. However, the accuracy order of the approximation to the derivative which is attained by two different kinds of numerical fluxes may be degraded

$$\tilde{u}'_1 = \frac{1}{h}(\tilde{u}_{3/2} - \tilde{u}_{1/2}) = \frac{1}{h}(S_{3/2} - S_{1/2}) + \mathcal{O}(h^3) = u'(x_1) + \mathcal{O}(h^3).$$

This means that the approximation of the derivatives at point x_1 is only third-order, which will cause the overall accuracy to be fourth-order at most according to the conclusion in [18]. In fact, Pirozzoli has proposed a boundary treatment for a fifth-order upwind conservative compact scheme as below [14]

$$\tilde{u}_{1/2} = \frac{1}{4}u_0 + \frac{13}{12}u_1 - \frac{5}{12}u_2 + \frac{1}{12}u_3, \quad (3.1a)$$

$$18\tilde{u}_{i-1/2} + 36\tilde{u}_{i+1/2} + 6\tilde{u}_{i+3/2} = 2u_{i-1} + 38u_i + 20u_{i+1}, \quad i = 1, \dots, N-1, \quad (3.1b)$$

$$\tilde{u}_{N+1/2} = -\frac{1}{4}u_{N-3} + \frac{13}{12}u_{N-2} - \frac{13}{12}u_{N-1} + \frac{25}{12}u_N. \quad (3.1c)$$

The scheme above is applied for right running waves. As for the left running waves, the scheme could be attained symmetrically. For a nonlinear problem, a flux splitting

$$B = \begin{bmatrix} 77/60 & -43/60 & 17/60 & -1/20 & & \\ 67/2 & 49/2 & 1/2 & & & \\ 3/2 & 67/2 & 49/2 & 1/2 & & \\ & \ddots & \ddots & \ddots & \ddots & \\ & & 3/2 & 67/2 & 49/2 & 1/2 \\ & -1/20 & 17/60 & -43/60 & 77/60 & 1/5 \\ & 1/5 & -21/20 & 137/60 & -163/60 & 137/60 \end{bmatrix}.$$

(ii) $U' = \frac{1}{h}CU$, here

$$C = \begin{bmatrix} -1 & 1 & & & \\ & \ddots & \ddots & & \\ & & -1 & 1 & \end{bmatrix}.$$

Then the semi-discrete approximation to (2.11) is

$$U_t = -\frac{c}{h}CA^{-1}(BU+b). \tag{3.3}$$

The asymptotic stability condition for this equation, which is necessary for the stability of long-time integration, is that all eigenvalues of matrix $P = -CA^{-1}B$ contain no positive real parts. Fig. 2 shows the eigenvalue spectra of the matrix P for $N = 50, 200, 400$. It is obvious that all eigenvalues are on the left side of the imaginary axis for these different node points, which means that the asymptotic stability condition is satisfied. The eigenvalue spectrum of P in the case of periodic boundary is also plotted with the solid line in the figure. The eigenvalues with the presence of boundary treatment (Eq. (3.2)) lie inside the region of the spectrum for periodic boundary condition, indicating that this boundary treatment stabilizes the overall numerical scheme.

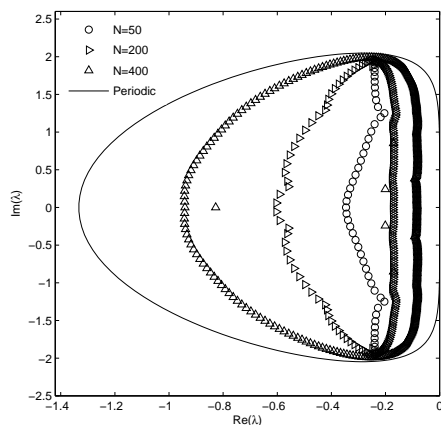


Figure 2: Spectrum of P for $N=50, 200, 400$ and the periodic condition.

3.3 Stability of the full discretization

A proper time scheme should be implemented to complete the numerical algorithm. In the present work, the fourth-order non-TVD Runge-Kutta scheme [12] is employed, which could be written as

$$\begin{aligned} U^{(1)} &= U^n + \frac{1}{2}\Delta t L(U^n), & U^{(2)} &= U^n + \frac{1}{2}\Delta t L(U^{(1)}), & U^{(3)} &= U^n + \Delta t L(U^{(2)}), \\ U^{n+1} &= \frac{1}{3}(-U^n + U^{(1)} + 2U^{(2)} + U^{(3)}) + \frac{1}{6}\Delta t L(U^{(3)}), \end{aligned}$$

where L is the spatial operator.

The stability of the full discretization will be carried out by utilizing von Neumann analysis which is appropriate for periodic problem. For the non-periodic case, this analysis could give a heuristic result and a matrix method would be more rigorous. However, in the previous subsection, the boundary scheme imposed shows better stability than periodic boundary treatment, which ensures the practical applicability of a von Neumann analysis. The spatial discretization could be expressed as the relation (2.10), named as transfer function. The amplification factor for the full discretization is

$$g(\kappa) = \left[1 + (-i\sigma\tilde{\kappa}) + \frac{1}{2}(-i\sigma\tilde{\kappa})^2 + \frac{1}{6}(-i\sigma\tilde{\kappa})^3 + \frac{1}{24}(-i\sigma\tilde{\kappa})^4 \right], \quad (3.4)$$

where $\sigma = c\Delta t/h$ is the Courant number, and $\tilde{\kappa}$ is given by Eq. (2.10). In Fig. 3, $g(\kappa)$ is plotted in polar coordinates for several values of κ . The von Neumann stability requires that the condition $|g(\kappa)| \leq 1$ is satisfied for $|\kappa| \leq \pi$. From the figure, the stable range of the Courant number is

$$\sigma \leq 1.421, \quad (3.5)$$

while the Courant number of upwind fifth-order compact scheme using biased stencil (Eq. (2.9) with $\alpha = -1$) with the same time integration method is $\sigma \leq 1.034$, which shows that the proposed scheme has a larger range of stability.

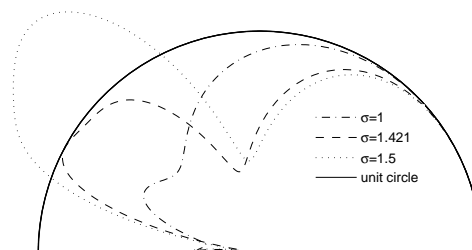


Figure 3: Amplification factor for different Courant numbers.

3.4 Convergence test

In this section, numerical tests on the convergence rate of the compact schemes including the boundary closures are performed. Two spatial discretizations, Eqs. (3.1) and (3.2) are tested. The linear advection equation Eq. (2.11) with advection speed $c = 1$ is considered, and the computational domain is $-1 \leq x \leq 1$. Here the time step is set as $\Delta t \sim \Delta x^{5/4}$, so that the fourth-order non-TVD Runge-Kutta method is effectively fifth-order.

In Tables 1 and 2, the errors and the convergence rates of these two schemes at $t = 1$ for the initial condition $u(x) = \sin(\pi x)$ and boundary condition $u(-1, t) = \sin(\pi(-1-t))$ are shown. The exact solution is $u_{exact} = \sin(\pi(x-t))$. In Tables 3 and 4, the initial condition and boundary condition are set to $u_0(x) = \sin^4(\pi x)$ and $u(-1, t) = \sin^4(\pi(-1-t))$ respectively, then the exact solution is $u_{exact} = \sin^4(\pi(x-t))$. It is clear that the spatial discretization (Eq. (3.1)) is actually fourth-order, because its boundary scheme is third-order in effect, as mentioned in the previous section. The proposed discretization (Eq. (3.2)) achieves fifth-order of accuracy which should be owed to a revised boundary implementation.

Table 1: Accuracy of Pirozzoli's scheme with initial condition $u_0(x) = \sin(\pi x)$.

Node number	L_1 error	L_∞ error	L_1 order	L_∞ order
32	2.505835e-004	3.916371e-004		
64	1.562229e-005	2.446612e-005	4.003614	4.000660
128	9.745787e-007	1.528567e-006	4.002684	4.000534
256	6.084378e-008	9.550225e-008	4.001597	4.000501

Table 2: Accuracy of the proposed scheme with initial condition $u_0(x) = \sin(\pi x)$.

Node number	L_1 error	L_∞ error	L_1 order	L_∞ order
32	4.315639e-005	7.767370e-005		
64	1.361171e-006	2.484943e-006	4.986654	4.966142
128	4.289418e-008	8.138891e-008	4.987922	4.932237
256	1.349553e-009	2.976401e-009	4.990228	4.773191

Table 3: Accuracy of Pirozzoli's scheme with initial condition $u_0(x) = \sin^4(\pi x)$.

Node number	L_1 error	L_∞ error	L_1 order	L_∞ order
32	8.563053e-003	1.562180e-002		
64	5.156418e-004	9.616685e-004	4.053684	4.021878
128	3.194247e-005	6.062458e-005	4.012821	3.987565
256	1.985865e-006	3.805754e-006	4.007637	3.993649

Table 4: Accuracy of the new scheme with initial condition $u_0(x) = \sin^4(\pi x)$.

Node number	L_1 error	L_∞ error	L_1 order	L_∞ order
32	5.614684e-003	1.045647e-002		
64	1.768152e-004	2.898994e-004	4.988891	5.172700
128	5.632880e-006	9.109440e-006	4.972225	4.992046
256	1.772034e-007	2.854653e-007	4.990394	4.995975

4 Coupling with WENO scheme

High-order linear schemes can perform well in smooth region, but for problems involving discontinuities these schemes produce oscillations whose amplitude does not decrease when the computational grids are refined. Of course, compact schemes mentioned in the previous section suffer from this drawback. Shock capturing mechanism, such as TVD compact schemes, weighted compact schemes, and hybrid schemes, should be added in order to cure this deficiency. In hybrid methods, compact schemes are used in smooth region while shock capturing methods are adopted only near the discontinuities. Therefore, they are more efficient than other nonlinear compact schemes. The hybrid methodology of Ren et al. [15] is adopted in this paper and will be briefly introduced. As the compact sub-scheme employed in their hybrid scheme is just the fifth-order compact scheme using upwind biased stencil corresponding to Eq. (2.9) with $\alpha = -1$, it will be replaced by the proposed compact scheme (Eq. (2.14)) in the following description.

This hybrid scheme is considered as the weighted average of two schemes: the compact fifth-order upwind scheme and the WENO scheme. For the left running waves, the compact scheme is

$$\frac{5}{12}\tilde{f}_{i-1/2} + \tilde{f}_{i+1/2} + \frac{1}{4}\tilde{f}_{i+3/2} = \frac{1}{24}f_{i-1} + \frac{67}{72}f_i + \frac{49}{72}f_{i+1} + \frac{1}{72}f_{i+2}, \quad (4.1)$$

which is just the proposed scheme in this work as the coefficient of $\tilde{f}_{i+1/2}$ is set to be 1. The shock capturing scheme is

$$\begin{aligned} \tilde{f}_{i+1/2} = & \frac{1}{6}\omega_0(2f_{i-2} - 7f_{i-1} + 11f_i) + \frac{1}{6}\omega_1(-f_{i-1} + 5f_i + 2f_{i+1}) \\ & + \frac{1}{6}\omega_2(2f_i + 5f_{i+1} - f_{i+2}), \end{aligned} \quad (4.2)$$

where ω_k is the nonlinear weight and the formulas can be referred to [12]. As for the right running waves, the two schemes can be attained by symmetry. For nonlinear problems, flux-splitting procedure should be employed and the Roe splitting with entropy fix is adopted in this hybrid method.

The weight of the compact scheme is $\sigma_{j+1/2}$ while that of the WENO scheme is $(1 - \sigma_{j+1/2})$. Here $\sigma_{j+1/2}$ is given by

$$\sigma_{j+1/2} = \min\left(1, \frac{r_{j+1/2}}{r_c}\right),$$

where

$$r_{j+1/2} = \min(r_j, r_{j+1}),$$

and

$$r_j = \frac{|2\Delta f_{j+1/2}\Delta f_{j-1/2}| + \varepsilon}{(\Delta f_{j+1/2})^2 + (\Delta f_{j-1/2})^2 + \varepsilon}, \quad \Delta f_{j+1/2} = f_{j+1} - f_j, \quad \varepsilon = 0.001.$$

The shock capturing scheme which is more time-consuming will only be applied for points near the discontinuities with this choice of weight.

For Euler equations, a characteristic decomposition approach is employed which is more accurate than the component approach. But the characteristic-wise compact scheme will lead to block-tri-diagonal systems of linear equations which will increase the computational cost. For more details, please refer to [15].

5 Numerical investigation

In this section, numerical investigation will be carried out to test the capability of the proposed scheme, called as ComCU5 here. For comparison, some schemes are also tested, including the fifth-order upwind compact scheme (Eq. (2.9) with $\alpha = -1$), the sixth-order central compact scheme (Eq. (2.9) with $\alpha = 0$), WENO scheme in [19], called as ComU5, ComC6, and WENO-Z respectively. The hybrid method is only applied for the last test case because there is a shock in that problem.

5.1 Two-dimensional rotation

This test case is the rotation of a Gaussian profile [20], given by

$$\phi(x, y) = \exp\left(-\frac{r^2}{2\sigma^2}\right),$$

with

$$r = \sqrt{(x - x_c)^2 + (y - y_c)^2},$$

where (x_c, y_c) is the center point of the profile and σ is a constant. In this case, the computational domain is $[0, 30] \times [0, 30]$, and $(x_c, y_c) = (15, 22.5)$, $\sigma = 1$. The governing equation for the motion of ϕ is given by

$$\frac{\partial \phi}{\partial t} + \frac{\partial (u\phi)}{\partial x} + \frac{\partial (v\phi)}{\partial y} = 0,$$

where $u = -\Omega(y - y_0)$ and $v = \Omega(x - x_0)$. $\Omega (= 2\pi/360)$ is the rotating angular velocity. The axis of the rotation (x_0, y_0) is $(15, 15)$ in this case. The profile will keep the original shape during the rotation. After one full rotation cycle, the distortion of the initial profile will reflect the capability of the numerical schemes.

ComCU5, ComU5, ComC6 and WENO-Z are tested on a uniform grid of 41×41 with a time step of $\Delta t = 0.25$. Fig. 4 shows the exact solution (initial profile) and numerical results. From the figure, the result of WENO-Z exhibits a serious damping of the Gaussian profile while that of ComC6 shows obvious oscillation. The two upwind compact schemes can preserve the profile well, while the profile of the ComCU5 is slimmer and closer to the initial profile than that of ComU5. The peak values of these profiles are listed

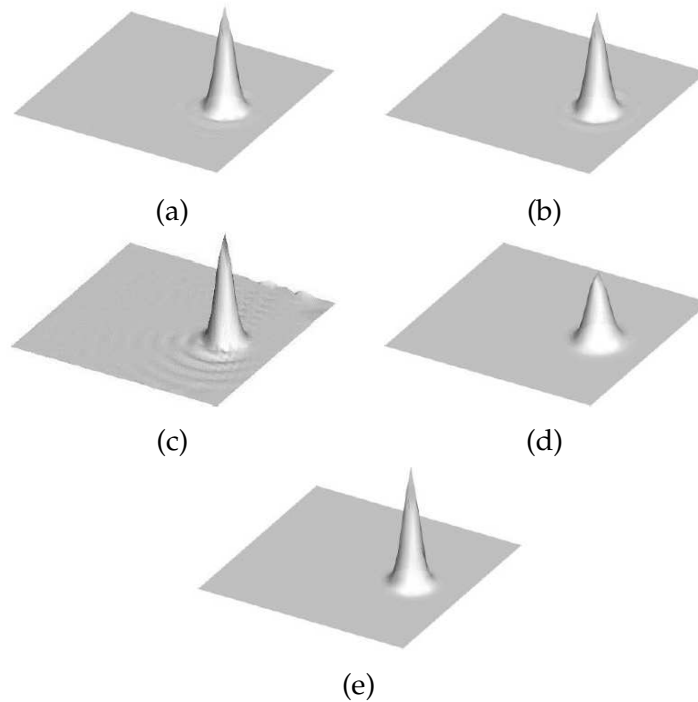


Figure 4: Perspective view of the initial profile and numerical results: (a) ComCU5; (b) ComU5; (c) ComC6; (d) WENO-Z; (e) initial profile.

in Table 5. In this table, it is obvious that ComC6 gets the highest peak value while ComCU5 ranks the second. Overall, the proposed scheme (ComCU5) gives the best profile shape, as compared with the initial profile.

Table 5: The peak value in the profile.

Method	ComCU5	ComU5	ComC6	WENO-Z	Exact
Peak value	0.884	0.846	0.921	0.587	1

5.2 Advection of an isentropic vortex

This test will validate the capability of the proposed scheme for long-time evolution. In this problem, an isentropic vortex convects in an inviscid free stream. The state of the mean flow is given by $(\rho, u, v, p) = (1, 1, 0, 1)$. The vortex can be described as a perturbation to the velocity (u, v) , temperature $T = p/\rho$, and entropy $S = \ln(p/\rho^\gamma)$ of the mean flow and it is denoted by the tilde values

$$\begin{aligned}
 u' &= \varepsilon \tau e^{\alpha(1-\tau^2)} \sin\theta, & v' &= -\varepsilon \tau e^{\alpha(1-\tau^2)} \cos\theta, \\
 S' &= 0, & T' &= -\frac{(\gamma-1)\varepsilon^2 e^{2\alpha(1-\tau^2)}}{4\alpha\gamma},
 \end{aligned}$$

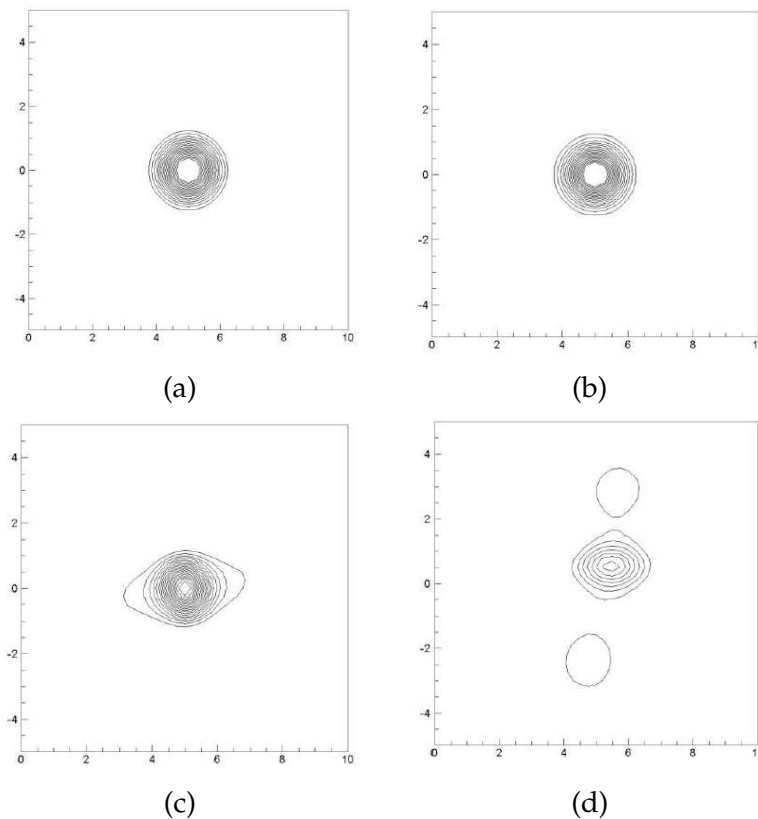


Figure 5: Density contours of the convecting vortex at $t=0, 100, 400$ and 1000 using ComU5, equally spaced 18 contours, $0.91 \sim 0.99$.

where $\tau = r/R$, $r = \sqrt{(x-x_c)^2 + (y-y_c)^2}$. Here ε indicates the strength of the vortex, α controls the decay rate of the vortex, and r is the critical radius for which the vortex has the maximum strength. These parameters are set as $\varepsilon = 0.3$, $R = 0.5$, $\alpha = 0.204$.

The computational domain is set as $[0,10] \times [-5,5]$ and the coordinates of the center of initial vortex is $(x_c, y_c) = (5,0)$. The mesh size is 41×41 and the time step size is set to 0.04 . Periodic boundary conditions in both directions are implemented. This vortex will return to the original position every non-dimensional time interval of $\Delta t = 10$. When the time elapsed for $m\Delta t$ (m is an integer), by comparing the vortex shape of the numerical results with the initial one, the dissipative character of the scheme could be evaluated.

Two upwind compact schemes, ComCu5 and ComC5, are tested. The density contours of the results of $t=0, 100, 400$ and 1000 are shown in Figs. 5 and 6. As seen in Fig. 5, when $t=100$, the shape of vortex can be maintained well while the shape of $t=400$ shows obvious distortion. The number of contour lines of $t=1000$ are less than those of other ones because the lowest density has achieved 0.962 as region of the contours is $0.91 \sim 0.99$. This means that the vortex has been seriously damped. However, in Fig. 6 when $t=1000$,

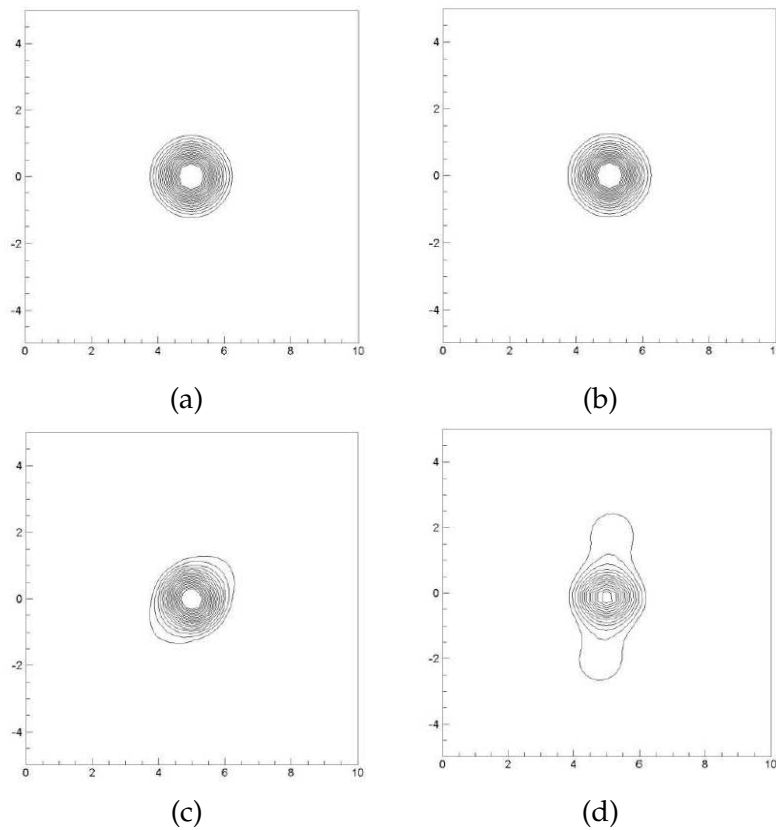


Figure 6: Density contours of the convecting vortex at $t=0, 100, 400$ and 1000 using ComCU5, equally spaced 18 contours, $0.91 \sim 0.99$.

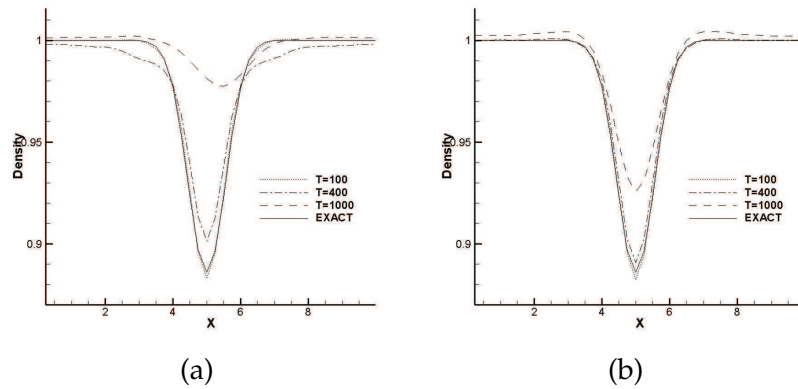


Figure 7: Density distributions of the convecting vortex along the center line at $t=0, 100, 400$ and 1000 , (a) ComU5, (b) ComCU5.

the shape of vortex is closer to the initial one than that in Fig. 5. This should be attributed to less dissipation of the scheme ComCu5. The density distributions of computational

results along the center line are plotted in Fig. 7, from which the same conclusion can be drawn clearly.

Furthermore, the result of stability of the full discretization in subsection 3.3 is also validated. According to our numerical results, in this test case, the maximum time step sizes of ComC5 and ComCU5 for stable computation are 0.070 and 0.098 respectively. The ratio of these two values is very close to the ratio of the two maximum Courant numbers which is 1.034/1.421. Therefore, this numerical result proves that ComCU5 has a larger range of stability than ComU5.

5.3 Shock-entropy wave interaction

This is a problem of one-dimensional Euler equation with the initial condition:

$$(\rho, u, p) = \begin{cases} (3.857143, 2.629369, 10.33333), & -5 \leq x < -4, \\ (1 + 0.2\sin 5x, 0, 1.0), & -4 \leq x \leq 5. \end{cases}$$

In this problem, an $M = 3$ shock wave interacts with a sine entropy wave of a density $\rho = 0.2$, which will generate a number of shocklets and fine scales of structures. The hybrid scheme proposed in this article with $r_c = 0.3$ is tested. For comparison, Ren et al.'s

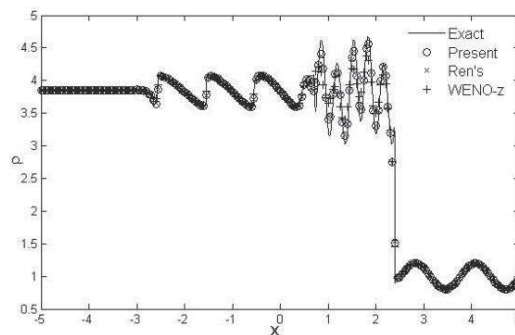


Figure 8: Shock-entropy wave interaction: distribution of density for $N = 200$.

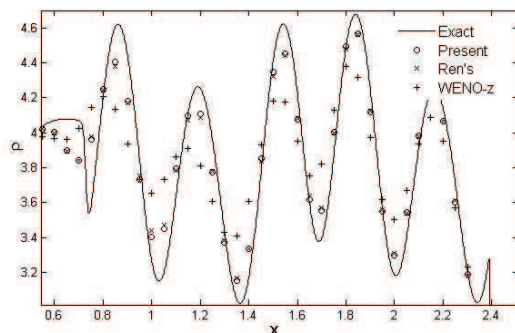


Figure 9: Enlarged portion of Fig. 8.

hybrid scheme ($r_c=0.3$) and WENO-Z are also tested. Fig. 8 provides the density profiles at $t = 1.8$ with $N = 200$. The solid line in the figure means "exact solution" attained by WENO5 scheme with 4000 nodes. Fig. 9 shows an enlarged portion of Fig. 8. From these figures, although WENO-Z scheme can capture the post-shock entropy waves fairly well, it performs worse than these two hybrid schemes. The present hybrid scheme performs the best, which should be owed to the small dissipation of the proposed compact scheme.

6 Conclusions

A fifth-order conservative upwind compact scheme using a centered stencil has been proposed in this work. Following the process in [10], the scheme is derived such that the dissipation error is smaller than the dispersive errors and is large enough for robustness of the scheme. Compared with the fifth-order conservative upwind compact scheme using an upwind biased stencil (named as ComU5 here), this compact scheme is less dissipative and has a larger range of stability. Since the boundary treatment of Pirozzoli [14] cannot maintain the accuracy order of the inner conservative compact scheme, a proper boundary scheme ensuring the convergence order of the whole spatial discretization has also been proposed. Convergence tests on the linear advection equation validate the fifth-order accuracy of the proposed scheme including the boundary closures. For problems with high gradient, the hybrid methodology of Ren et al. has been adopted [15].

Three test cases are employed to validate the property of the proposed scheme. Firstly, numerical test on two-dimensional rotation problem shows that the proposed compact scheme is low-dissipative and robust. Secondly, numerical results on advection of vortex show that it performs well for long time evolution because of its low-dissipative property. Besides, the range of stability of this scheme larger than that of ComU5 is also validated. Lastly, results on shock-entropy wave interaction give an example for hybrid methods and verify the low-dissipative property of the proposed scheme again.

Acknowledgements

This research was supported by National Natural Science Foundation of China (91130030). The authors are grateful to Dr. Jie Wu for his help on the manuscript.

References

- [1] C. LEE AND Y. SEO, *A new compact spectral scheme for turbulence simulations*, J. Comput. Phys., 183 (2002), pp. 438–469.
- [2] S. NAGARAJAN, S. K. LELE AND J. H. FERZIGER, *A robust high order compact method for large eddy simulation*, J. Comput. Phys., 191 (2003), pp. 392–419.
- [3] J. A. EKATERINARIS, *Implicit high-resolution compact schemes for gas dynamics and aeroacoustics*, J. Comput. Phys., 156 (1999), pp. 272–299.

- [4] A. LERAT AND C. CORRE, *A residual-based compact scheme for the compressible Navier-Stokes equations*, J. Comput. Phys., 170 (2001), pp. 642–675.
- [5] C. K. W. TAM AND J. C. WEBB, *Dispersion-relation-preserving finite difference schemes for computational acoustics*, J. Comput. Phys., 107 (1993), pp. 262–281.
- [6] D. W. ZINGG, *Comparison of high-accuracy finite-difference methods for linear wave propagation*, SIAM J. Sci. Comput., 22 (2000), pp. 476–502.
- [7] S. K. LELE, *Compact difference schemes with spectral-like resolution*, J. Comput. Phys., 103 (1992), pp. 16–42.
- [8] A. I. TOLSTYKH AND M. V. LIPAVSKII, *On performance of methods with third- and fifth-order compact upwind differencing*, J. Comput. Phys., 140 (1998), pp. 205–232.
- [9] C. K. W. TAM, J. C. WEBB AND Z. DONG, *A study of the short wave components in computational acoustics*, J. Comput. Acoust., 1 (1993), pp. 1–30.
- [10] X. ZHONG, *High-order finite-difference schemes for numerical simulation of hypersonic boundary-layer transition*, J. Comput. Phys., 144 (1998), pp. 662–709.
- [11] N. A. ADAMS AND K. SHARIF, *A high-resolution hybrid compact-ENO scheme for shock-turbulence interaction problems*, J. Comput. Phys., 127 (1996), pp. 27–51.
- [12] G. S. JIANG AND C.-W. SHU, *Efficient implementation of weighted ENO schemes*, J. Comput. Phys., 126 (1996), pp. 202–228.
- [13] A. JAMESON, W. SCHMIDT AND E. TURKEL, *Numerical solutions of the Euler equations by finite volume methods using Runge-Kutta time-stepping schemes*, AIAA-81-1259, (1981).
- [14] S. PIROZZOLI, *Conservative hybrid compact-WENO schemes for shock-turbulence interaction*, J. Comput. Phys., 178 (2001), pp. 81–117.
- [15] Y. X. REN, M. LIU AND H. X. ZHANG, *A characteristic-wise hybrid compact-WENO scheme for solving hyperbolic conservation laws*, J. Comput. Phys., 192 (2003), pp. 365–386.
- [16] D. KIM AND J. H. KWON, *A high-order accurate hybrid scheme using a central flux scheme and a WENO scheme for compressible flowfield analysis*, J. Comput. Phys., 210 (2005), pp. 554–583.
- [17] Q. ZHOU, Z. YAO, F. HE AND M. SHEN, *A new family of high-order compact upwind difference schemes with good spectral resolution*, J. Comput. Phys., 227 (2007), pp. 1306–1339.
- [18] B. GUSTAFSSON, *The convergence rate for difference approximations to mixed initial boundary value problems*, Math. Comput., 29 (1975), pp. 396–406.
- [19] R. BORGES, M. CARMONA, B. COSTA AND W. S. DON, *An improved weighted essentially non-oscillatory scheme for hyperbolic conservation laws*, J. Comput. Phys., 227 (2008), pp. 3191–3211.
- [20] Z. WANG AND G. P. HUANG, *An essentially nonoscillatory high-order Pade-type (ENO-Pade) scheme*, J. Comput. Phys., 177 (2002), pp. 37–58.